NASA/TM-20250005468

E-Band GaN MMIC Power Amplifier for Multi-Gigabit Satellite Communications and Lunar Surface Wireless Links

Rainee N. Simons and Ian R. Nemitz
Glenn Research Center, Cleveland, Ohio

Mansoor K. Siddiqui
Northrop Grumman Aerospace Systems, Redondo Beach, California

Scott Niemiec
Rohde & Schwarz USA, Inc., Belvidere, Illinois

September 2025

NASA STI Program Report Series

Since its founding, NASA has been dedicated to the advancement of aeronautics and space science. The NASA scientific and technical information (STI) program plays a key part in helping NASA maintain this important role.

The NASA STI program operates under the auspices of the Agency Chief Information Officer. It collects, organizes, provides for archiving, and disseminates NASA's STI. The NASA STI program provides access to the NTRS Registered and its public interface, the NASA Technical Reports Server, thus providing one of the largest collections of aeronautical and space science STI in the world. Results are published in both non-NASA channels and by NASA in the NASA STI Report Series, which includes the following report types:

- TECHNICAL PUBLICATION.
  Reports of completed research or a major significant phase of research that present the results of NASA programs and include extensive data or theoretical analysis. Includes compilations of significant scientific and technical data and information deemed to be of continuing reference value. NASA counterpart of peer-reviewed formal professional papers but has less stringent limitations on manuscript length and extent of graphic presentations.

- TECHNICAL MEMORANDUM.
  Scientific and technical findings that are preliminary or of specialized interest, e.g., quick release reports, working papers, and bibliographies that contain minimal annotation. Does not contain extensive analysis.

- CONTRACTOR REPORT.
  Scientific and technical findings by NASA-sponsored contractors and grantees.

- CONFERENCE PUBLICATION.
  Collected papers from scientific and technical conferences, symposia, seminars, or other meetings sponsored or cosponsored by NASA.

- SPECIAL PUBLICATION.
  Scientific, technical, or historical information from NASA programs, projects, and missions, often concerned with subjects having substantial public interest.

- TECHNICAL TRANSLATION.
  English-language translations of foreign scientific and technical material pertinent to NASA's mission.

Specialized services also include organizing and publishing research results, distributing specialized research announcements and feeds, providing information desk and personal search support, and enabling data exchange services.

For more information about the NASA STI program, see the following:

- Access the NASA STI program home page at http://www.sti.nasa.gov

NASA/TM-20250005468

E-Band GaN MMIC Power Amplifier for Multi-Gigabit Satellite Communications and Lunar Surface Wireless Links

Rainee N. Simons and Ian R. Nemitz
Glenn Research Center, Cleveland, Ohio

Mansoor K. Siddiqui
Northrop Grumman Aerospace Systems, Redondo Beach, California

Scott Niemiec
Rohde & Schwarz USA, Inc., Belvidere, Illinois

National Aeronautics and
Space Administration

Glenn Research Center
Cleveland, Ohio 44135

September 2025

Acknowledgments

The figures for this NASA TM are archived under E-20341.

This report contains preliminary findings,
subject to revision as analysis proceeds.

Level of Review: This material has been technically reviewed by technical management.

This report is available in electronic form at https://www.sti.nasa.gov/ and https://ntrs.nasa.gov/

NASA STI Program/Mail Stop 050
NASA Langley Research Center
Hampton, VA 23681-2199

E-Band GaN MMIC Power Amplifier for Multi-Gigabit Satellite Communications and Lunar Surface Wireless Links

Rainee N. Simons and Ian R. Nemitz
National Aeronautics and Space Administration
Glenn Research Center
Cleveland, Ohio 44135

Mansoor K. Siddiqui
Northrop Grumman Aerospace Systems
Redondo Beach, California 90278

Scott Niemiec
Rohde & Schwarz USA, Inc.
Belvidere, Illinois 61008

Abstract

In this paper, we present the performance characteristics of an E-band (70-75 GHz) gallium nitride (GaN) high electron mobility transistor (HEMT) monolithic microwave integrated circuit (MMIC) based high power amplifier (HPA). The results presented include output power, Gain, power added efficiency (PAE), noise figure (NF), 3rd-order intermodulation distortion (IMD) products, RMS error vector magnitude (EVM), spectral efficiency, spectrum, and spectral regrowth for OQPSK, 8PSK, 16APSK, 32APSK, 16QAM, 32QAM, 64QAM, and 128QAM waveforms. The intended application of the HPA is for multi-gigabit satellite communications, lunar surface communications, and terrestrial backhaul networks.

Introduction

The demand for multi-gigabit satellite communication links and terrestrial fixed wireless links is ever increasing because of the emerging 5G/6G wireless communications. This need can be met by exploiting the available spectrum at E-band. The E-band spectrum ranging from 71-76 GHz and 81-86 GHz is designated by the FCC for satellite communication downlinks and uplinks, respectively, as well as for high-capacity terrestrial fixed wireless backhaul networks, as illustrated in Figure 1. In the case of terrestrial links, the 71-76 GHz and 81-86 GHz ranges are known as the lower and upper E-band spectrum. The rational for selecting the E-band frequencies for the above links are spectrum availability, capability to support large channel bandwidths required for future terabit-per-second (Tbps) SATCOM, reusability of the spectrum made possible because of highly directive pencil beam antennas that lowers co-frequency interference, small size and low mass of hardware, and lower spectrum licensing cost (Ref. 1).

E-band terrestrial link experiments to characterize rain attenuation, depolarization, scintillation, and gaseous absorption effects of Earth's atmosphere are reported in References 2 and 3. In addition, field testing of an E-band high speed, long range, multi-channel wireless datalink is reported in Reference 4. The link made use of four 2 GHz wide channels with 64QAM modulation in each of the lower and upper E-band spectrum. Using a combination of frequency and polarization multiplexing, the link supported 65 Gbps error free bidirectional user data rates over a 16 km distance. Thus, demonstrating optical fiber equivalent speed (Ref. 4).

The design of an E-band beacon/transponder system payload on a geostationary Earth orbit (GEO) satellite for a propagation measurement campaign to acquire relevant statistical data on the effect of Earth's atmospheric on satellite communication downlink signals is reported in Reference 5. Furthermore, link budget analysis for LEO and GEO satellites is presented in Reference 6. Moreover, an initial link budget estimate for GEO satellites is provided in Reference 7. Lastly, in Reference 8, the launching of a 6U CubeSat into low Earth orbit (LEO) with an E-band transmitter as a payload is reported. The goal is to demonstrate a space-to-Earth E-band downlink. Depending on the modulation/coding technique, the transmitter is designed to support signals requiring 700 MHz to 5 GHz bandwidth and data rates up to 10 Gbps. The on-orbit performance of the payload transmitter is under evaluation (Ref. 8).

To enable E-band multi-gigabit satellite communications in the future, new HPA technologies are required. HPAs with high output power, lower mass and size, excellent linearity, and capability to operate in the harsh environment of space are desired. High electron mobility transistor (HEMT) based monolithic microwave integrated circuit (MMIC) power amplifier chips fabricated on epitaxially grown gallium nitride on high resistivity silicon carbide (GaN-on-SiC) wafers, imparts several significant benefits over prior gallium arsenide (GaAs) and silicon (Si) technologies. These include higher operating voltage, higher output power density,

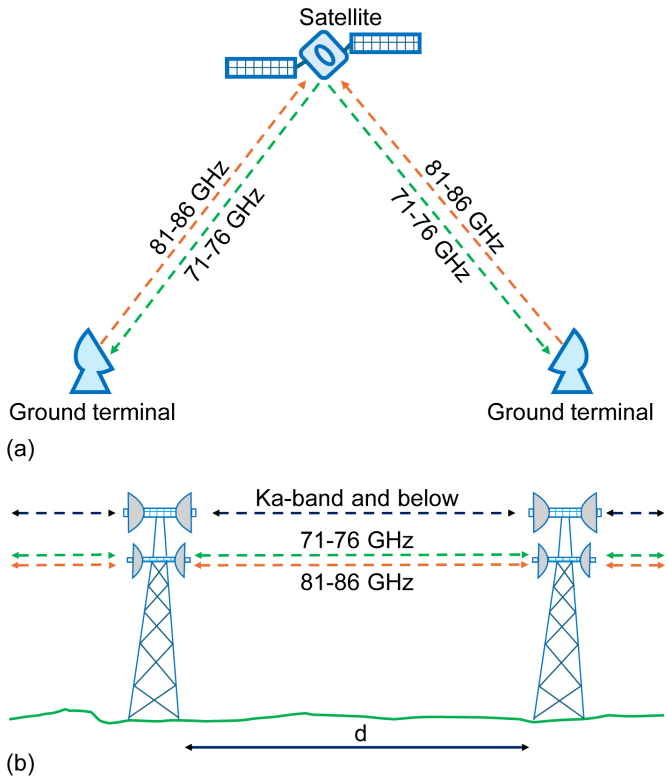

Figure 1.—E-band links. (a) Space-to-Earth links. (b) Terrestrial point-to-point links. The distance between the towers is d.

higher channel operating temperatures, and radiation hardness (Refs. 9, 10, 11, and 12). Beyond terrestrial, LEO, and GEO applications, E-band systems owing to their compact size and low mass could also benefit NASA's Artemis lunar missions. Future missions may require multichannel wireless data links to support a network of science instruments, habitats, landers, and terrain vehicles or rovers operating on the lunar surface. The development of E-band GaN HEMT MMIC based HPAs for satellite downlinks and 5G backhaul applications are reported in References 1, 13, and 14.

This paper builds on our prior and ongoing efforts in GaN HEMT MMIC based HPAs. Recently, we demonstrated at Ka-band a prototype of a dual band switched GaN HEMT based MMIC HPAs that operates either at 25-28 GHz or at 28-31 GHz frequency bands, depending on the requirement at any moment. The HPA is developed for user spacecraft terminals to support interoperability with multiple commercial SATCOM networks (Ref. 15). Additionally, we investigated the benefits offered by GaN HPA's performance characteristics for user spacecraft cognitive radio platforms that can learn from the environment in which they are operating, and adaptively and dynamically change the operating parameters (Ref. 16). Furthermore, we demonstrated a prototype GaN HPA that operates over the 23.15-23.55 GHz frequency band for future lunar proximity communication forward links, which are planned between assets located in the lunar orbit and lunar surface, cross-links between lunar relays, and links to science mission spacecraft (Ref. 17). Moreover, we demonstrated a protype HPA, based on a waveguide 4-port magic-tee as a 2-way power combiner to combine the output from two GaN MMIC power amplifier (PA) chips (Ref. 18). Still more, we presented the results of an experimental study conducted to compare the microwave performance of a prototype distributed HPA with the above dual band switched HPA for wideband applications (Ref. 19). Lastly, at E-band (76-81 GHz), we demonstrated a protype HPA for vehicular radar for lunar surface mobility applications (Ref. 20).

In this paper we extend our investigations to the characterization of an E-band HPA over the frequency range of 70-75 GHz for future multi-gigabit space-to-Earth satellite communication links, lunar surface communications, and terrestrial backhaul networks. The results presented here include the E-band HPA output power, Gain, power added efficiency (PAE), noise figure (NF), 3rd-order intermodulation distortion (IMD) products, RMS error vector magnitude (EVM), spectral efficiency, spectrum, and spectral regrowth for OQPSK, 8PSK, 16APSK, 32APSK, 16QAM, 32QAM, 64QAM, and 128QAM waveforms. The rational for performing the above measurements and their significance to the design of satellite communication systems are discussed in our prior publications (Refs. 15 to 20).

E-Band GaN HEMT MMIC Based HPA Architecture and Brief Set of Specifications

HPA Architecture

The HPA consists of three multi-stage MMIC chips that are cascaded and packaged to form a compact module. To couple signals in and out from the underside of the module, two WR-12 waveguide 90° E-plane bends are used as the input and output ports. In addition, to conveniently interface the input/output ports with standard waveguide test and measurement equipment, it is preferred to have ports that are co-linear during characterization. Furthermore, for waste heat removal the module is attached to an aluminum heat sink. The heat sink is constructed in such a manner to accommodate the above waveguide bends. The overall packaged assembly is illustrated in Figure 2.

Brief Set of Specifications

- GaN HEMT MMICs: Northrop Grumman Space Park, GaN015 process
- Module Saturated output power (P_{sat}): 30 dBm (1 W) (CW)
- Max input RF drive power: 4 to 5 dBm
- Bandwidth: 70 to 75 GHz
- PAE: 4 to 5 percent
- Small signal gain: 29 to 31 dB
- Power gain: 25 to 26 dB

- Module input/output return loss: <10.0 dB
- Gain flatness over full bandwidth: < ±1 dB
- Input/output ports: WR-12 waveguide
- Max drain bias quiescent levels:
  - Max V_{d1} and V_{d2} = 29 V
  - Max I_{d1} = 620 mA
  - Max I_{d2} = 180 mA
- Nominal gate quiescent voltage:
  - V_{g1} = –3.5 V
  - V_{g2} = –3.5 V
- Nominal gate quiescent current:
  - I_{g1} = 23 µA
  - I_{g2} = 500 nA

HPA E-Band Performance Validation

The test set up for measuring the P_{out}, Gain, and PAE of the E-band GaN HEMT MMIC based HPA is shown in Figure 3. The set up consists of Rohde & Schwarz (R&S) SMW200A Vector Signal Generator (VSG), R&S FSW Signal and Spectrum Analyzer (SAA), R&S FE110ST and FE110SR Frontend (Tx & Rx) Extensions (70-110 GHz), R&S NXR Power Meter, R&S NRP 90S 3-Path Diode Power Sensor, Keysight N6705C DC Power Analyzer, Hughes 45726H-1000 Precision Direct Reading Rotary Vane Attenuator, and Eravant 20 dB Directional Coupler.

Output Power, Gain, and Power Added Efficiency

The measured P_{out}, Gain, and PAE as a function of the unmodulated input drive power P_{in} to the HPA at 70, 72.5, and 75 GHz are presented in Figure 4 to Figure 6, respectively. At the center frequency of 72.5 GHz and when P_{in} is equal to –0.9 dBm, the output power compresses by 1 dB. The operating drain voltages (V_d) and gate voltages (V_g) are indicated in the figure caption. The measured unmodulated saturated output power (P_{sat}) and the peak PAE as a function of the frequency are presented in Figure 7.

Noise Figure

The test set up for measuring the NF and the measured results are presented in Figure 8 and Figure 9, respectively. The NF is less than 9.4 dB across the 70 to 75 GHz band.

3rd-Order Intermodulation Products

The test set up for measuring the 3rd-order IMD products and the measured IMD are presented in Figure 10 and Figure 11, respectively. The data indicates that the output 3rd-order intercept point (OIP3) at 72.5 GHz is on the order of 36 dBm.

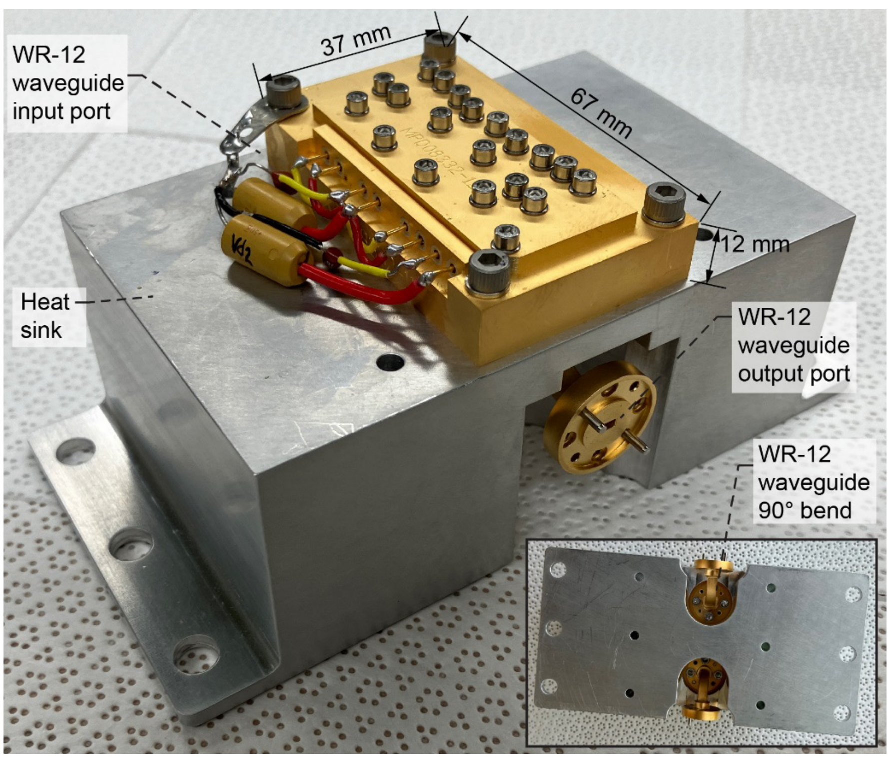

Figure 2.—Packaged E-band GaN HEMT MMIC based high power amplifier module mounted on a heat sink. Inset shows two waveguide 90° E-plane bends attached to opposite side of package and serves as input/output ports for testing. V_{ds1} = V_{ds2} = 28 V, V_{gs1} = V_{gs2} = –3.5 V, I_{ds1} = 500 mA (max.), and Ids2 = 200 mA (max.).

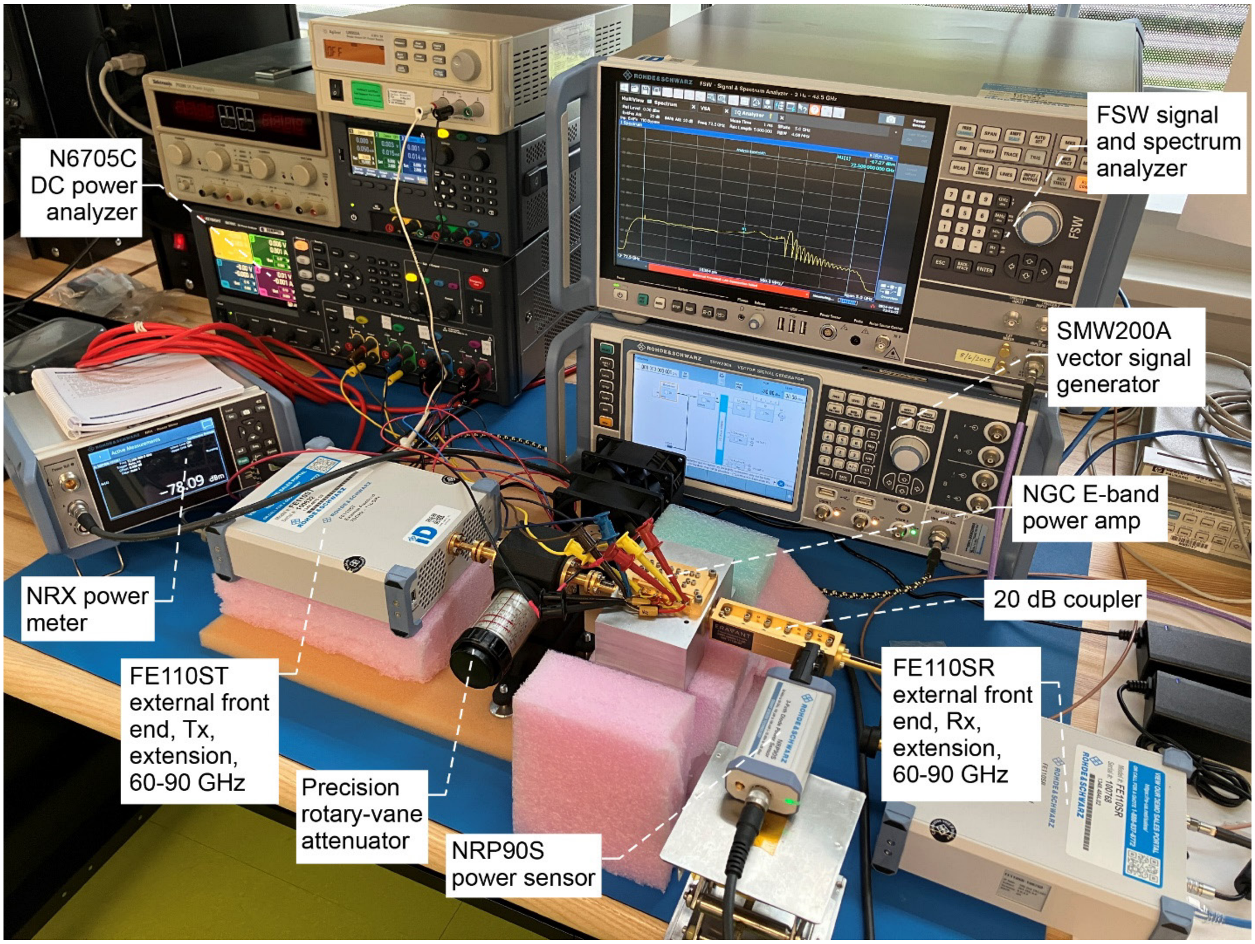

Figure 3.—E-band test set up for measuring the P_{out}, gain, and PAE.

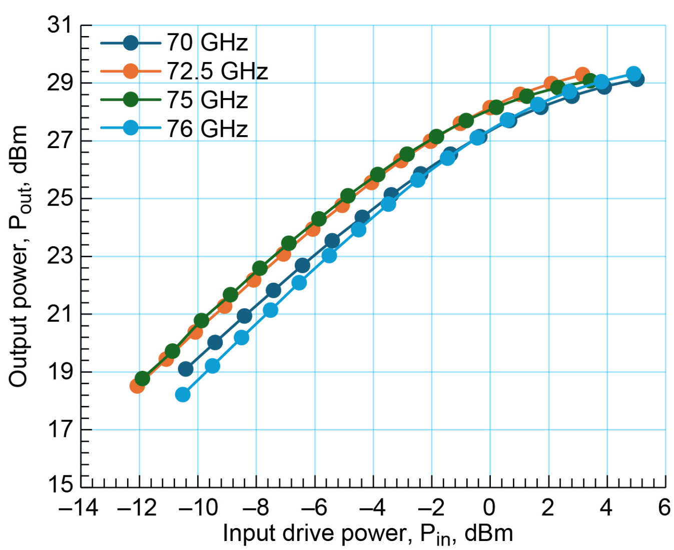

Figure 4.—Measured P_{out} vs. P_{in} for E-band GaN MMIC HPA. $V_{ds1} = V_{ds2} = 28$ V, $V_{gs1} = V_{gs2} = –3.5$ V, $I_{ds1} = 500$ mA (max.), and $I_{ds2} = 200$ mA (max.).

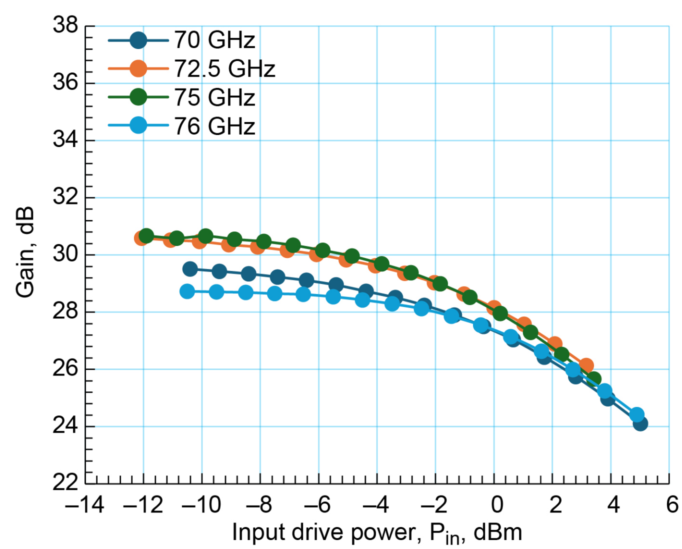

Figure 5.—Measured gain vs. P_{in} for E-band GaN MMIC HPA. $V_{ds1} = V_{ds2} = 28$ V, $V_{gs1} = V_{gs2} = –3.5$ V, $I_{ds1} = 500$ mA (max.), and $I_{ds2} = 200$ mA (max.).

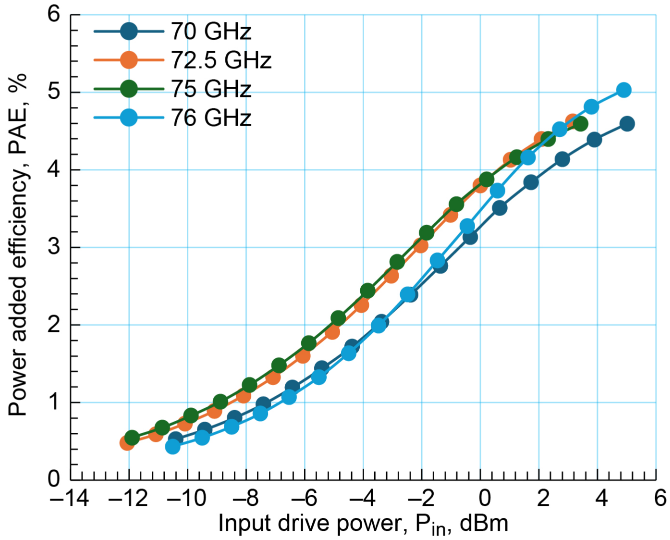

Figure 6.—Measured PAE vs. P_{in} for E-band GaN MMIC HPA. $V_{ds1} = V_{ds2}$ = 28 V, $V_{gs1} = V_{gs2}$ = –3.5 V, I_{ds1} = 500 mA (max.), and I_{ds2} = 200 mA (max.).

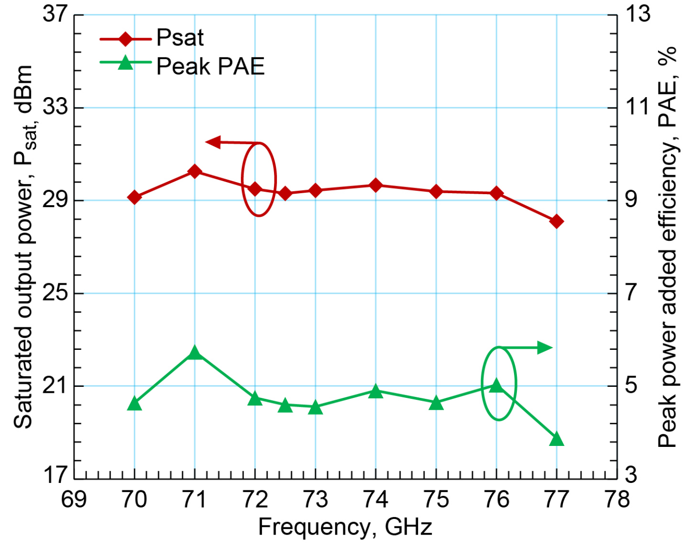

Figure 7.—Measured P_{sat} and peak PAE vs. frequency for E-band GaN MMIC HPA. $V_{ds1} = V_{ds2}$ = 28 V, $V_{gs1} = V_{gs2}$ = –3.5 V, I_{ds1} = 500 mA (max.), and I_{ds2} = 200 mA (max.).

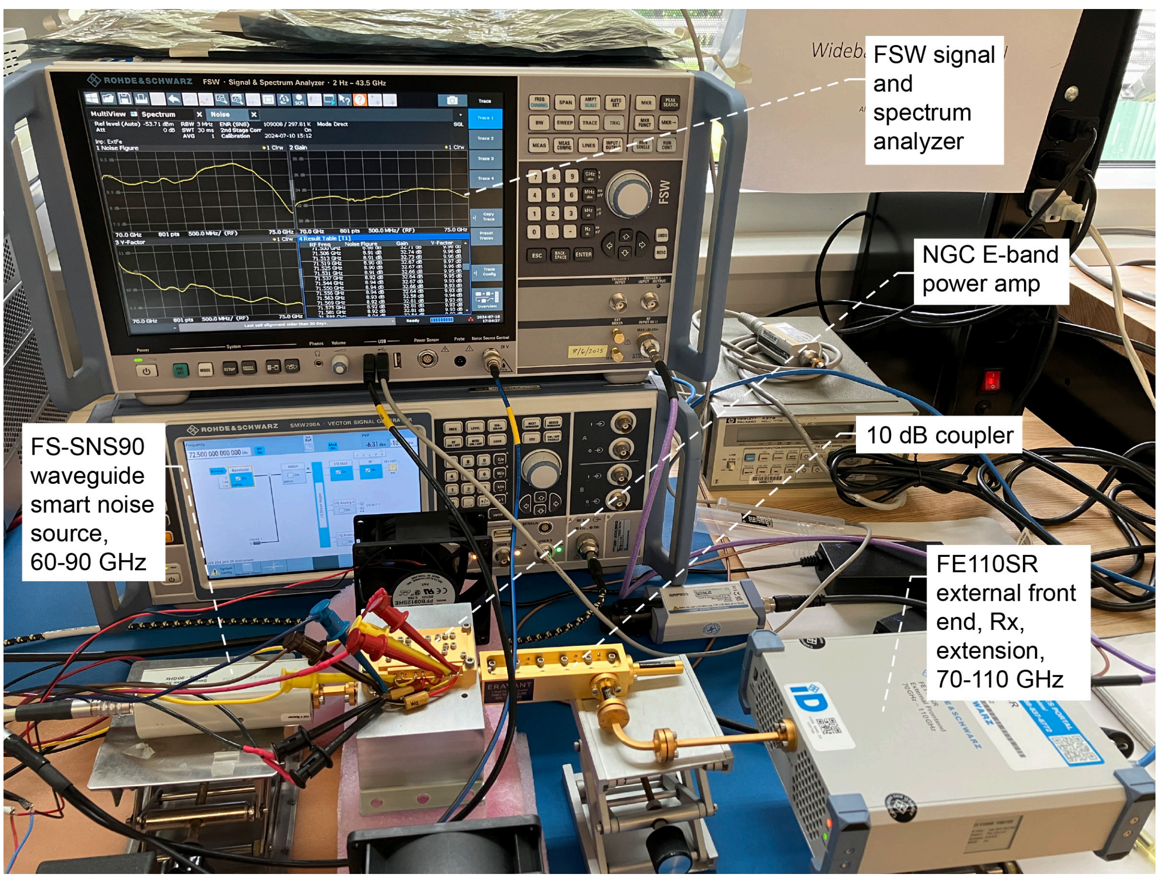

Figure 8.—E-band test set up for measuring the NF.

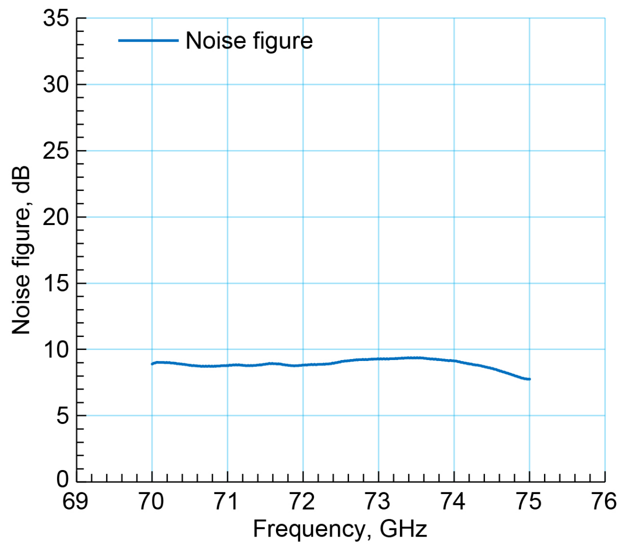

Figure 9.—Measured NF vs. frequency of E-band GaN MMIC HPA. $V_{ds1} = V_{ds2} = 28$ V, $V_{gs1} = V_{gs2} = –3.5$ V, $I_{ds1} = 500$ mA (max.), and $I_{ds2} = 200$ mA (max.).

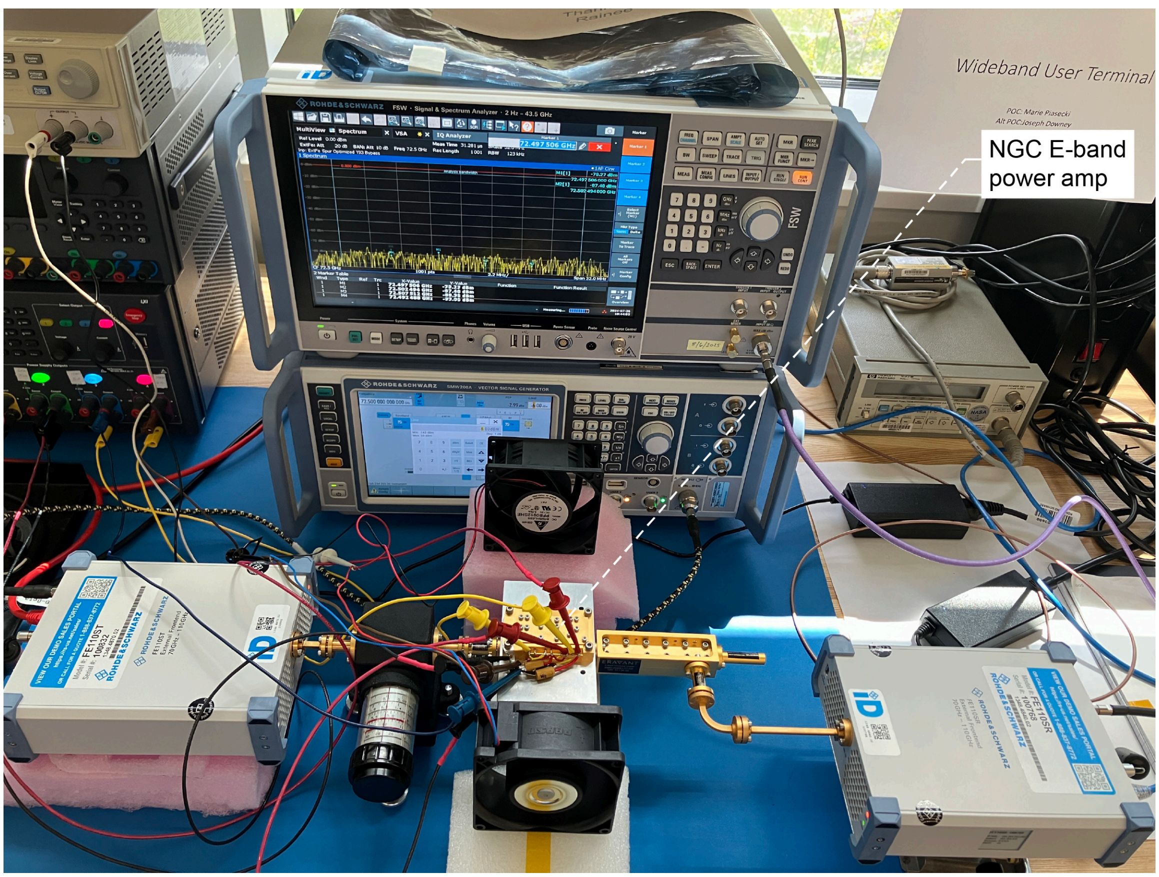

Figure 10.—E-band test set up for measuring the 3rd-order intermodulation distortion, RMS EVM, and spectrum.

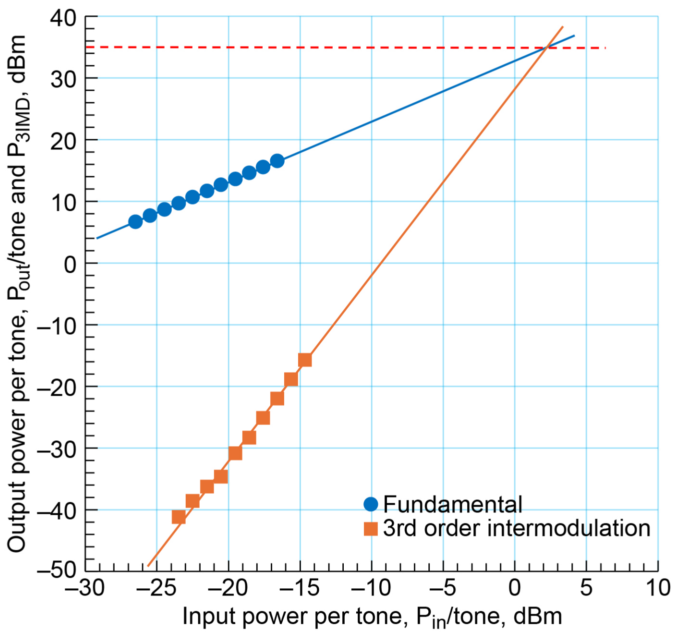

Figure 11.—Measured output power per tone (P_{out}/tone) and 3rd-order intermodulation distortion vs. input power per tone (P_{in}/tone) for E-band GaN MMIC HPA. Carrier frequency is 72.5 GHz, tone frequencies are 72.5 GHz±2.5 MHz, and tone spacing is 5 MHz. $V_{ds1} = V_{ds2} = 28$ V, $V_{gs1} = V_{gs2} = –3.5$ V, $I_{ds1} = 500$ mA (max.), and $I_{ds2} = 200$ mA (max.).

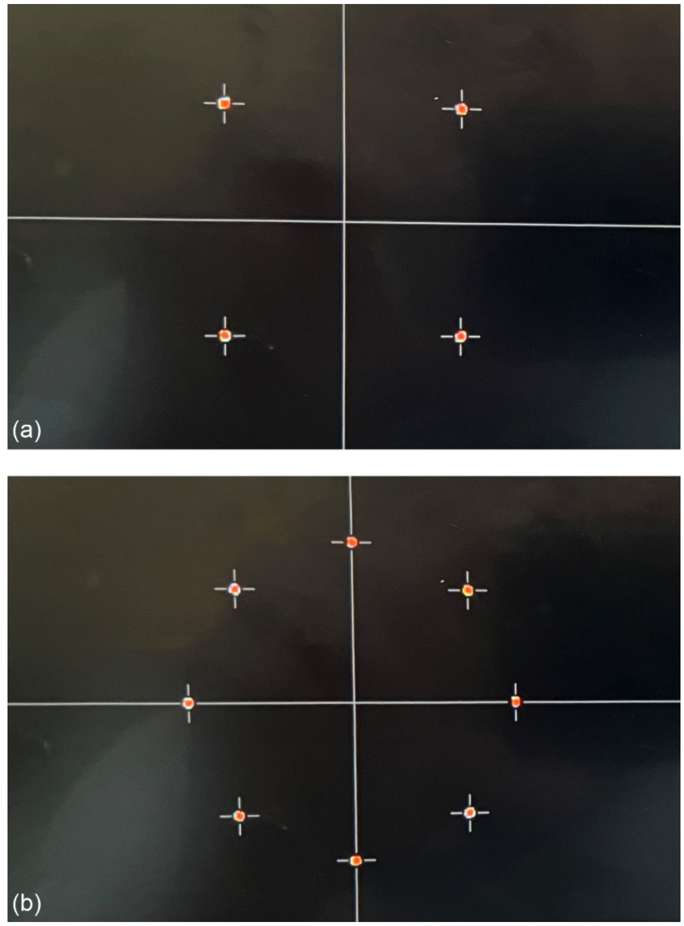

Figure 12.—The waveform constellations. (a) OQPSK. (b) 8PSK.

RMS Error Vector Magnitude (EVM), Spectral Efficiency, Spectrum, and Spectral Regrowth

Offset QPSK and 8PSK Waveforms

The waveform constellations for OQPSK and 8PSK generated by the VSG are shown in Figure 12. The measured RMS EVM as a function of P_{in} with modulation, as observed on the SSA at 72.5 GHz, is presented in Figure 13. Since 8PSK has all the constellation points on a circle of constant magnitude throughout the modulation process, the 8PSK waveform is less susceptible to non-linearities and hence has better EVM performance than OQPSK waveform. As the waveform switches from OQPSK to 8PSK, the spectral efficiency improves from 2 to 3 bits/s/Hz. The measured spectrum, when P_{in} is such that the RMS EVM is 5%, is shown in Figure 14. Additionally, for both waveforms the out-of-band spectral regrowth measured at 1-symbol rate (200 MHz) away from f_0 (that is at 72.7 GHz) are indicated by a red dash line in Figure 14.

16APSK and 32APSK Waveforms

The waveform constellations for 16APSK and 32APSK are shown in Figure 15 and the measured RMS EVM as a function of P_{in} at 72.5 GHz is presented in Figure 16. As the waveform switches from 16APSK to 32APSK, the spectral efficiency improves from 4 to 5 bits/s/Hz. The measured spectrum, when P_{in} is such that the RMS EVM is 5%, is shown in Figure 17. Additionally, for both waveforms the out-of-band spectral regrowth measured at 1-symbol rate (200 MHz) away from f_0 (that is at 72.7 GHz) are indicated by a red dash line in Figure 17.

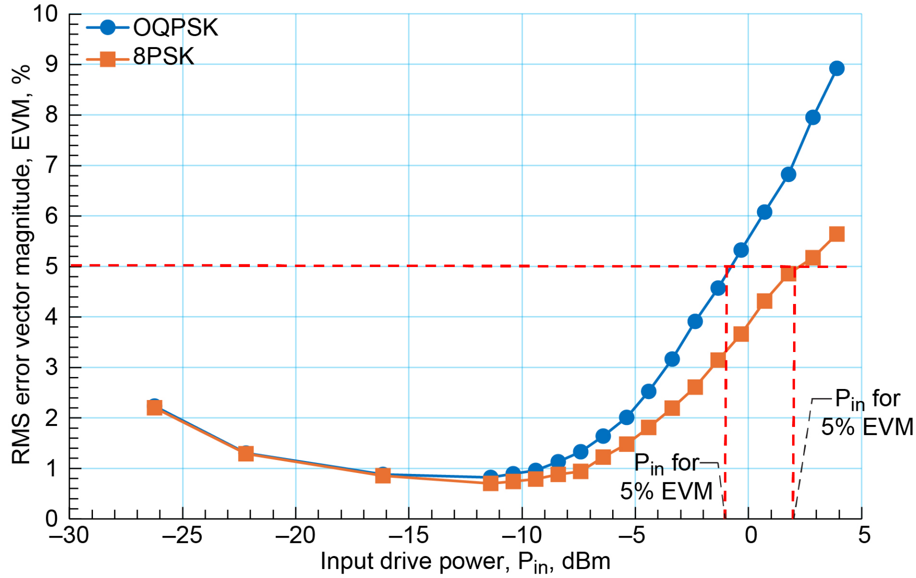

Figure 13.—Measured RMS error vector magnitude (EVM) vs. P_{in} at carrier frequency of 72.5 GHz. Symbol rate is 200 Msymbols per second and square root raised cosine (SRRC) filter is set to 0.35.

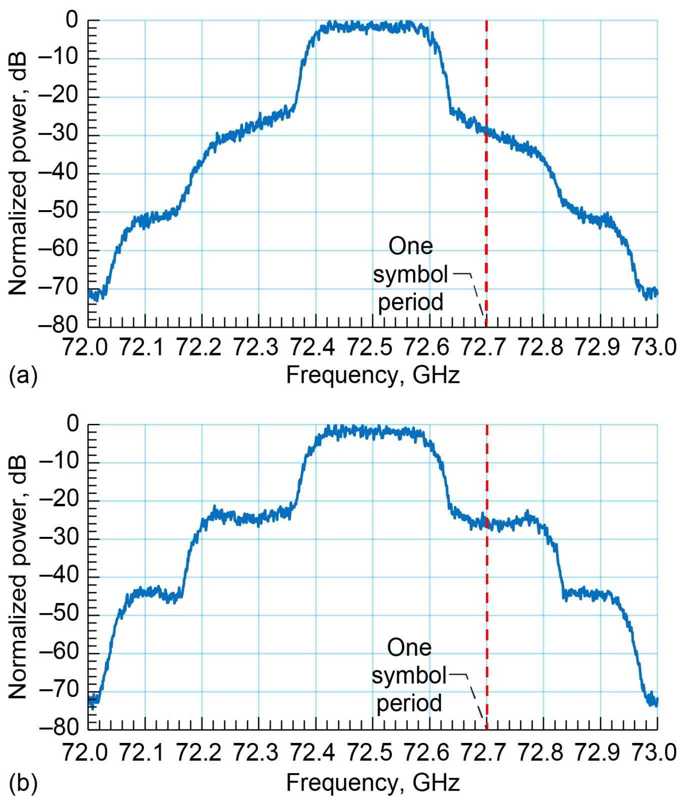

Figure 14.—Measured spectrum of waveforms. Carrier frequency is 72.5 GHz, symbol rate is 200 Msymbols per second, SRRC filter is set to 0.35, EVM = 5%, bandwidth is 225 MHz. (a) OQPSK, P_{in} = –1.16 dBm. (b) 8PSK, P_{in} = 1.95 dBm.

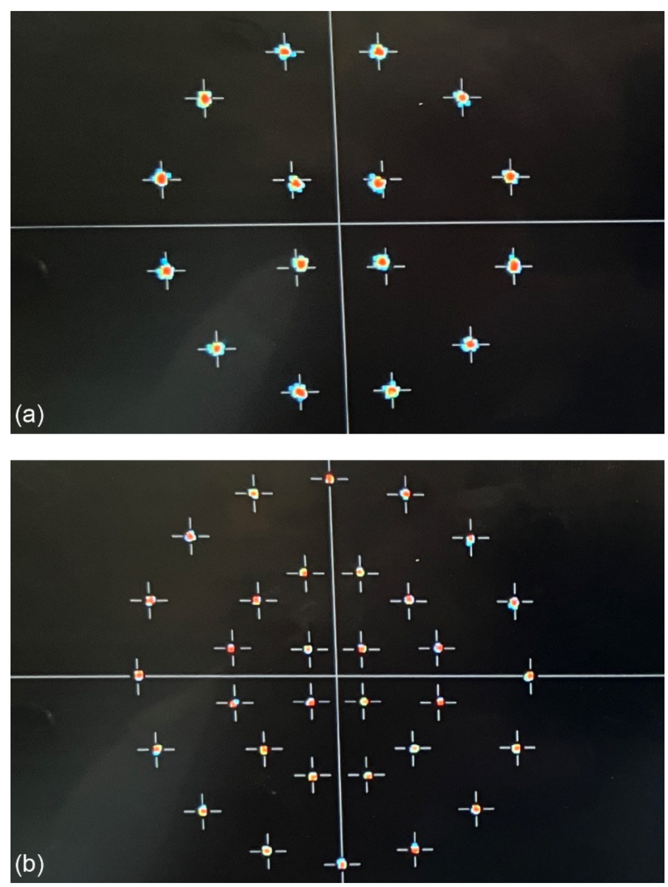

Figure 15.—The waveform constellations. (a) 16APSK. (b) 32APSK.

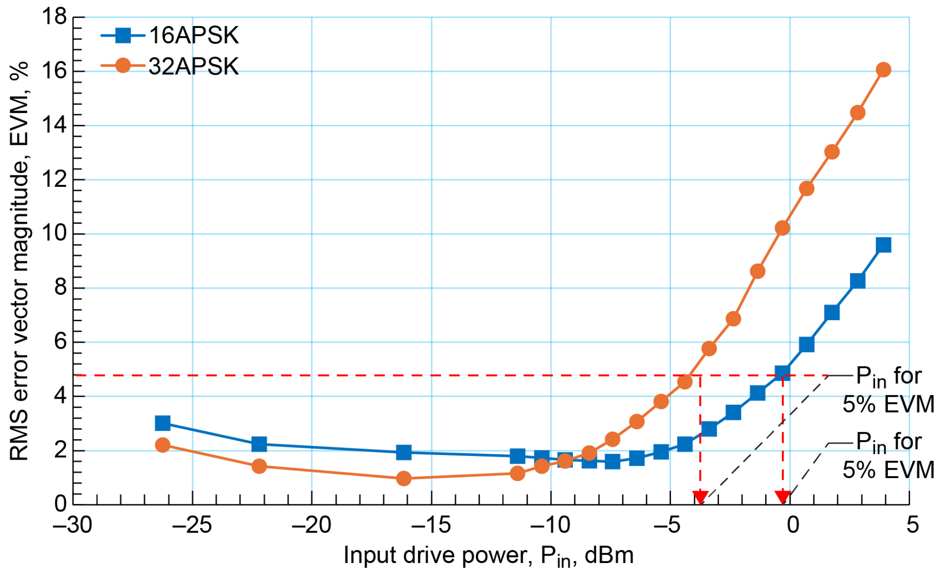

Figure 16.—Measured RMS error vector magnitude (EVM) vs. P_{in} at carrier frequency of 72.5 GHz. Symbol rate is 200 Msymbols per second and square root raised cosine (SRRC) filter is set to 0.35.

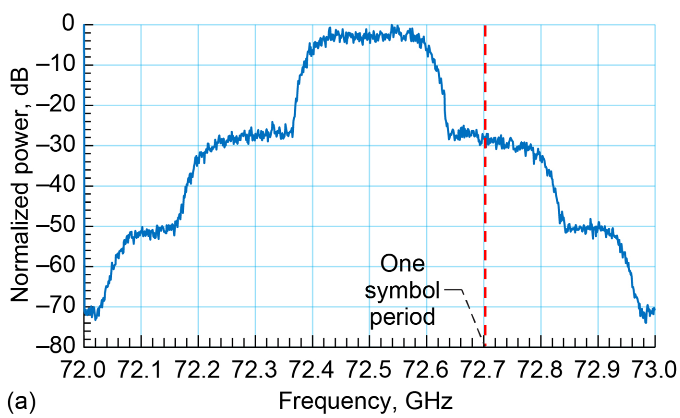

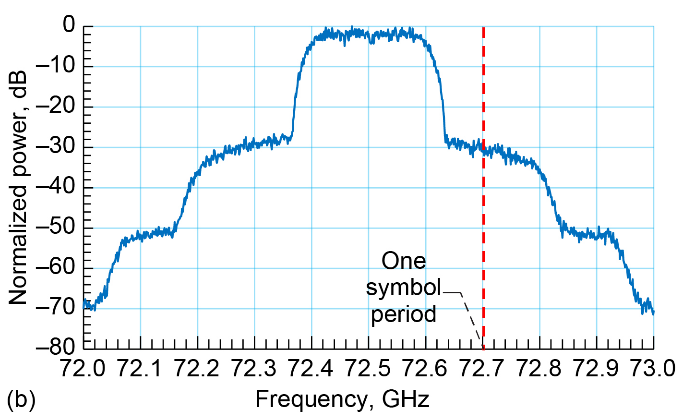

Figure 17.—Measured spectrum of the waveforms. Carrier frequency is 72.5 GHz, symbol rate is 200 Msymbols per second, SRRC filter is set to 0.35, EVM = 5%, bandwidth is 225 MHz. (a) 16APSK, P_{in} = -1.66 dBm. (b) 32APSK, P_{in} = –3.81 dBm.

16QAM, 32QAM, 64QAM, and 128QAM Waveforms

The waveform constellations for 16QAM, 32QAM, 64QAM, and 128QAM are shown in Figure 18 and the measured RMS EVM as a function of P_{in} at 72.5 GHz is presented in Figure 19. As the waveform switches from 16QAM through 128QAM, the spectral efficiency improves from 4 to 7 bits/s/Hz. The measured spectrum, when P_{in} is such that the RMS EVM is 5%, is shown in Figure 20. Additionally, for all four waveforms the out-of-band spectral regrowth measured at 1-symbol rate (200 MHz) away from f_0 (that is at 72.7 GHz) are indicated by a red dash line in Figure 20. The performance summary of the E-band GaN MMIC power amplifier is presented in Table I.

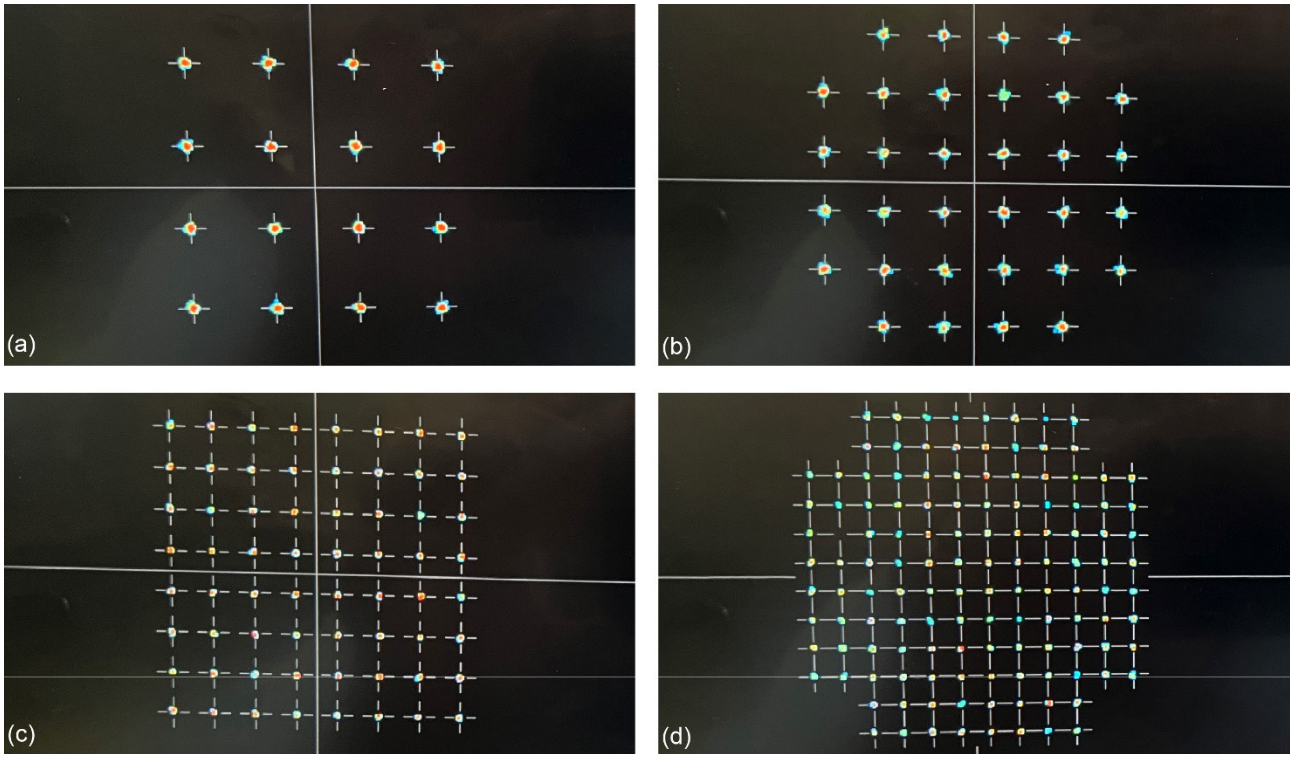

Figure 18.—The waveform constellations. (a) 16QAM. (b) 32QAM. (c) 64QAM. (d)128QAM.

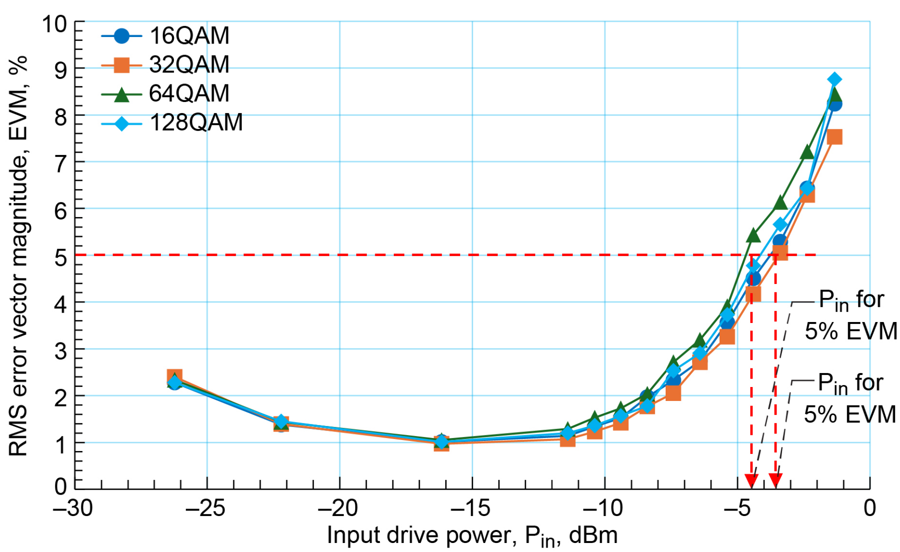

Figure 19.—Measured RMS EVM vs. P_{in} at carrier frequency of 72.5 GHz. Symbol rate is 200 Msymbols per second and square root raised cosine (SRRC) filter is set to 0.35.

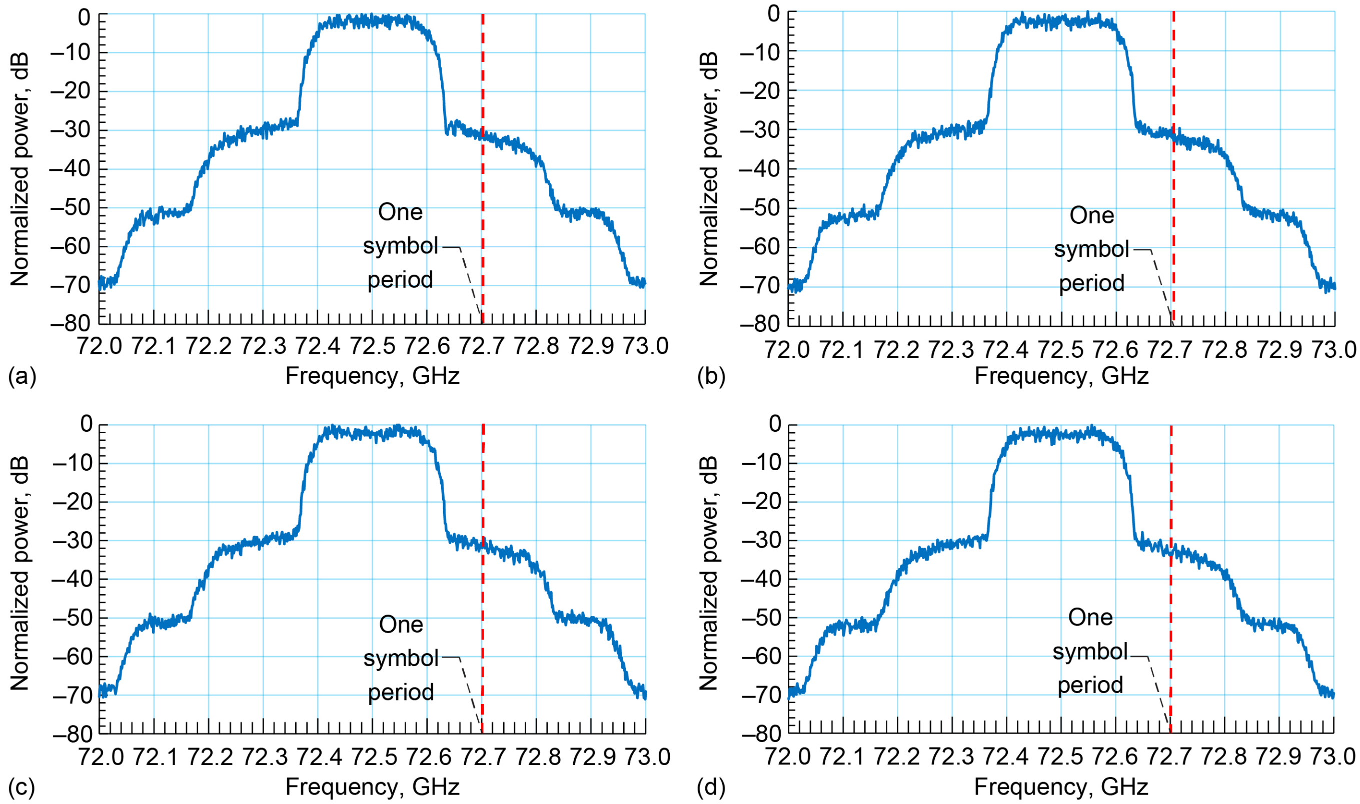

Figure 20.—Measured spectrum of waveforms. Carrier frequency is 72.5 GHz, symbol rate is 200 Msymbols per second, SRRC filter is set to 0.35, EVM = 5%, bandwidth is 225 MHz. (a) 16QAM, P_{in} = –3.79 dBm. (b) 32QAM, P_{in} = –3.38 dBm. (c) 64QAM, P_{in} = –4.65 dBm. (d) 128QAM, P_{in} = –4.29 dBm.

TABLE I.—PERFORMANCE SUMMARY OF E-BAND GaN MMIC POWER AMPLIFIER

Parameter	Measured value							
Frequency, GHz	70		72.5			75		
Small signal gain, dB	29.0		29.8			30.0		
Saturated output power, P_{sat}, dBm	29.0		29.3			29.1		
Peak Power Added Efficiency (PAE), %	4.6		4.6			4.6		
Gain at saturation or power gain, dB	24.1		26.1			25.7		
OIP3, dBm	--		36			----		
Noise figure, dB	7.8 to 9.4							
Waveform	OQPSK	8PSK	16APSK	32APSK	16QAM	32QAM	64QAM	128QAM
RMS EVM at 72.5 GHz, %	5	5	5	5	5	5	5	5
Corresponding out-of-band spectral regrowth at 72.5 GHz, dBc	25.2	23.4	26.2	27.1	29.0	30.2	29.2	31.7

Conclusions

A E-band (70-75 GHz) GaN HEMT MMIC based HPA is characterized by measuring the output power, gain, power added efficiency (PAE), noise figure (NF), 3rd-order intermodulation distortion (IMD) products, RMS error vector magnitude (EVM), spectral efficiency, spectrum, and spectral regrowth. No derating and no estimation of the HEMT junction temperature were performed. The above prototype HPA development is at technology readiness level of 4. The intended application of the HPA is for multi-gigabit satellite communications, lunar surface communications, and terrestrial backhaul networks.

References

1. A. Colzani, M. Fumagalli, A. Fonte, A. Traversa, and E. Ture, "Long-Reach E-band HPA for 5G Radio Link," *2022 52nd European Microwave Conference (EuMC)*, Milan, Italy, Sept. 27-29, 2022.
2. N.P. Tarasenko, S.A. Lane, D.A. Murrell, C. Christodoulou, J. Nessel, M. Zemba, and J. Houts, "W/V-band Terrestrial Link Experiment, an Overview," *2016 IEEE International Symposium on Antennas and Propagation (APSURSI)*, Fajardo, PR, June 26-July 1, 2016.
3. M. Zemba, J. Nessel, J. Houts, N. Tarasenko, S. Lane, and D. Murrell, "Preliminary Results from the AFRL-NASA W/V-band Terrestrial Link Experiment in Albuquerque, NM," *2016 IEEE International Symposium on Antennas and Propagation (APSURSI)*, Fajardo, PR, June 26-July 1, 2016.
4. K. Brown, A. Brown, T. Feenstra, D. Gritters, E. Ko, S. O'Connor, and M. Sotelo, "Long-Range Wireless Link with Fiber-Equivalent Data Rate," *2017 IEEE MTT-S International Microwave Symposium (IMS) Digest*, pp. 809-811, Honolulu, HI, June 4-9, 2017.
5. R.J. Acosta, J.A. Nessel, R.N. Simons, M.J. Zemba, J.R. Morse, and J. Budinger, "W/V-band RF Propagation Experiment Design," *Proceedings 18th Ka and Broadband Communications, Navigation, and Earth Observation Conference*, pp. 355-362, Ottawa, Canada, Sept. 24-27, 2012.
6. U.J. Lewark, J. Antes, J. Walheim, J. Timmermann, T. Zwick, and I. Kallfass, "Link Budget Analysis for Future E-band Gigabit Satellite Communication Links (71-76 and 81-84 GHz)," *Council of European Aerospace Societies (CEAS) Space Journal*, vol. 4, pp. 41-46, 14 Feb. 2013.
7. S. Morrar, "Using E-band for Wideband Satcom: Opportunities and Challenges," (Invited Paper), *Microwave Journal*, vol. 64, no. 8, pp. 22-32, Aug. 2021.
8. M. Kranz, M. Eggert, M. Koller, M. Lengowski, J. Meier, R. Muller, R. Schweigert, S. Klinkner, S. Haussmann, L. Manoliu, B. Schoch, I. Kallfass, A. Tessmann, R. Henneberger, and J. Freese, "One Year Satellite Operations of the E-band Technology Demonstration CubeSat EIVE," SSC24-WVII-06, *Proceedings of the 38th AIAA/USU Conference on Small Satellites*, Utah State University, UT, Aug. 1-8, 2024.
9. S. Din, M. Wojtowicz and M. Siddiqui, "High Power and High Efficiency Ka-Band Power Amplifier," *IEEE MTT-S International Microwave Symposium Digest*, Phoenix, AZ, May 17-22, 2015.
10. S. Din, A.M. Morishita, N. Yamamoto, C. Brown, M. Wojtowicz, and M. Siddiqui, "High-Power K-Band GaN PA MMICs and Module for NPR and PAE," *IEEE MTT-S International Microwave Symposium Digest*, Honolulu, HI, June 4-9, 2017.
11. P. Harati, B. Schoch, A. Tessmann, D. Schwantuschke, R. Henneberger, H. Czekala, T. Zwick, and I. Kallfass, "Is E-band Satellite Communication Viable?" *IEEE Microwave Magazine*, vol. 18, Issue 7, pp. 64-76, Nov.-Dec. 2017.
12. F. Medjdoub, K. Shinohara, F. Thome, J.S. Moon, E. Chumbes, M.T. Guidry, U. Mishra, E. Zanoni, M. Meneghini, G. Meneghesso, J.W. Pomeroy, T. Thingujam, and M. Kuball, "Emerging GaN Technologies for Next-Generation Millimeter-Wave Applications," *IEEE Microwave Magazine*, vol. 25, Issue 10, pp. 18-37, Oct. 2024.
13. B. Cimbili, C. Friesicke, F. van Raay, M. Bao, and R. Quay, "E-band Downlink GaN PA with a Homogeneous Output Power of 2.7W and a Peak PAE of 32.3%," *2023 18th European Microwave Integrated Circuits Conference (EuMIC)*, Berlin, Germany, Sept. 18-19, 2023.
14. B. Cimbili, M. Bao, C. Friesicke, and R. Quay, "E-band (71-to-86 GHz) GaN Power Amplifier with 4.37W Output Power and 18.5% PAE for 5G Backhaul," *2024 IEEE International Solid-State Circuits Conference (ISSCC) Digest of Technical Papers,* pp. 528-530, San Francisco, CA, Feb. 18-22, 2024.
15. R.N. Simons, J.A. Downey, B.L. Schoenholz, M.T. Piasecki, N.T. Pham, M.K. Siddiqui, and R.G. Bonnin, "Demonstration of a Switched Wideband GaN High-Power Amplifier for Future Space Missions," *2023 IEEE Space Hardware and Radio Conference,* Las Vegas, NV, Jan. 22-25, 2023.
16. R.N. Simons, A.M. Gannon, J.A. Downey, M.T. Piasecki, and B.L. Schoenholz, "Benefits of Ka-band GaN MMIC High Power Amplifiers with Wide Bandwidth and High Spectral/Power Added Efficiencies for Cognitive Radio Platforms," *2023 IEEE Cognitive Communications for Aerospace Applications Workshop (CCAAW)*, Cleveland, OH, June 20-22, 2023.
17. R.N. Simons, M.T. Piasecki, J.A. Downey, B.L. Schoenholz, M.K. Siddiqui, "Demonstration of GaN HEMT MMIC High-Power Amplifier for Lunar Proximity Communications," *2024 IEEE Space Hardware and Radio Conference*, San Antonio, TX, Jan. 21-24, 2024.
18. R.N. Simons, M.T. Piasecki, J.A. Downey, B.L. Schoenholz, "Spectrally Efficient GaN High-Power Amplifier for Lunar Communications," NASA/Technical Memorandum-20240012991, Nov. 2024 (Available at https://ntrs.nasa.gov).
19. R.N. Simons, M.T. Piasecki, J.A. Downey, B.L. Schoenholz, "Amplifier Output Power, Efficiency, Bandwidth, and Linearity: A Comparative Study of GaN Distributed versus Dual Band Switched Power Amplifiers," NASA/Technical Memorandum-20250001703, March 2025 (Available at https://ntrs.nasa.gov).
20. R.N. Simons, I.R. Nemitz, J.C. Soric, A.K. Brown, and N.J. Kolias, "E-Band GaN MMIC Power Amplifier for Vehicular Radar for Lunar Surface Mobility," *2025 IEEE International Symposium on Antennas and Propagation/North America Radio Science Meeting*, Ottawa, Canada, July 13-18, 2025.